Paper No.
403

CORROSION 95
The NACE International Annual Conference and Corrosion Show

SIMULTANEOUS RADIOLYSIS, ECP, AND CRACK GROWTH MODELING OF COMPONENTS IN BWR COOLANT SYSTEMS

Digby D. Macdonald and Tsung-Kuang Yeh
Center for Advanced Materials
The Pennsylvania State University
517 Deike Building
University Park, PA 16802

Arthur T. Motta
Department of Nuclear Engineering
The Pennsylvania State University
231 Sackett Building
University Park, PA 16802

ABSTRACT

An algorithm for assessing, theoretically, the effectiveness of hydrogen water chemistry (HWC) in Boiling Water Reactors (BWRs) is described. The algorithm, DAMAGE-PREDICTOR, contains facilities for estimating the concentrations of radiolysis products (in particular O_2, H_2, and H_2O_2), the electrochemical corrosion potential (ECP), and the kinetics of growth of a reference crack in sensitized Type 304SS, around the primary heat transport circuit (HTC) as a function of power level and the concentration of hydrogen added to the feedwater. The power level, in turn, determines various thermal-hydraulic input parameters and the neutron and gamma energy deposition rate in the core and near-core regions. These input parameters are estimated using well-established algorithms, and the simulations have been carried out for full power conditions for two reactors that differ markedly in their responses to HWC. DAMAGE-PREDICTOR, when calibrated against recirculation oxygen levels in one plant, is found to successfully account for various plant data from both reactors (including steam line oxygen and hydrogen levels, ECP values from remote autoclaves attached to the recirculation system, and in-core ECP data) using a single set of model parameter values.

Keywords: Boiling Water Reactor, hydrogen water chemistry, water radiolysis, stress corrosion cracking, ECP, crack growth rate.

INTRODUCTION

Incidences of Intergranular Stress Corrosion Cracking (IGSCC) and Irradiation-Assisted Stress Corrosion Cracking (IASCC) of stainless steel components in the primary heat transport circuits (HTCs) of Boiling Water Reactors (BWRs) are occurring with increasing frequency as the nation's nuclear power reactors age. In particular, concern has arisen over the cracking of BWR in-vessel components,

such as the core-shroud, upper plenum structure, jet pump, etc. Of considerable concern would be cracking of components in the lower plenum, which contains the control rod drives, because of the safety implications and because of the considerable cost of repair.

Perhaps the most promising solution to this problem is Hydrogen Water Chemistry (HWC) in which hydrogen (H_2) is added to the reactor feedwater so as to reduce the oxygen and hydrogen peroxide concentrations and ultimately the Electrochemical Corrosion Potential (ECP). However, this technique is not without problems, because the generation of mildly reducing conditions within the HTC results in the transfer of radioactive N^{16} to the steam phase in the form of nitrogen and/or ammonia, rather than remaining in the water (and hence in the primary circuit) as oxyanions of nitrogen that form under oxidizing conditions. The volatile ammonia is transported through the main steam line to the turbines and condensers, and the resulting radiation fields exact a high man-REM cost on the operator, which must be balanced against the potential benefits of HWC. Furthermore, it is not at all clear that HWC is effective in protecting some components against IGSCC and IASCC, particularly those in-vessel components that are exposed to high gamma and neutron fields. Importantly, the level of effectiveness appears to depend strongly on the particular reactor under consideration. Thus, Ruiz et al[1], using radiochemical modeling techniques, combined with recirculation line oxygen measurements, analyzed the responses of nine commercial BWRs to HWC. They showed that the ability of hydrogen added to the feedwater to reduce the oxygen in the recirculation system varied greatly from plant-to-plant. Similar models have also been developed in the past by other workers[2-5].

Macdonald et al[6,7], using Ruiz et al's calculated H_2, O_2, and H_2O_2 concentrations at various points around the primary HTC, estimated the ECP using a Mixed Potential Model (MPM). They found that HWC, as described by Ruiz et al[1], was not effective in displacing the ECP of many in-vessel components to sufficiently negative values to achieve protection as the hydrogen added to feedwater was increased. These components include the core and bypass structure, the upper plenum structures, and the downcomer. In some reactors, it was doubtful that HWC could protect the recirculation system and lower plenum, but in other reactors these components were predicted to be protected by displacement of the ECP to values more negative than -0.23 V_{SHE} [the value adopted by the Nuclear Regulatory Commission (NRC) as the critical potential for IGSCC]. Where comparisons could be made, the predictions of the MPM were in good agreement with ECP data measured in operating BWRs, thereby lending credence to the viability of ECP modeling via the MPM.

Since these initial studies, we have developed a water radiolysis code (RADIOCHEM), which we have combined with the MPM and a crack growth rate algorithm (CEFM)[8-12] to predict damage due to IGSCC and IASCC in BWR primary HTCs. The resultant code, DAMAGE-PREDICTOR, is largely deterministic in nature, in that the component models satisfy known physicochemical laws. The viability of this code is assessed by simulating the responses to HWC of the two reactors (Duane Arnold and Dresden-2) that were included in the original study of Ruiz et al[1]. We show that the calculations are internally consistent, in that a single set of parameters is able to described the responses of these two quite different BWRs to HWC.

THEORETICAL BASIS

The structure of the DAMAGE-PREDICTOR algorithm used in this analysis is illustrated in Figure 1. The main body of the algorithm is the water radiolysis model, which calculates the concentrations of radiolysis products from the decomposition of water due to neutron and gamma irradiation. The water radiolysis model (RADIOCHEM) makes use of chemical reactions coupled to fluid convection, in order to calculate the concentrations of the species at points around the heat transport circuit. After the species concentrations have been determined in the whole primary heat transport circuit, the ECP is calculated using the Mixed Potential Model (MPM) and the crack growth rate of a reference crack is also estimated using the Coupled Environment Fracture Model (CEFM). Auxiliary input parameters, such as flow velocity, coolant temperature, steam quality, and neutron and gamma dose rates in the coolant are obtained from running other available software packages or from Ruiz et al's work[1]. The nine regions of a BWR heat transport circuit that are specifically covered in this

study are illustrated schematically in Figure 2. The concentration of each species is calculated assuming transport in one dimension.

Water Radiolysis

The radiolysis of water in BWR heat transport circuits has long been recognized as the source of the approximately 200 ppb of oxygen that is found in the recirculation system under normal operating conditions. However, in order to explore the effectiveness of HWC, it is important that all radiolytic species distributions be calculated, since species other than oxygen are electroactive and hence will have an impact on the ECP and on the crack growth rate. In order to calculate the species concentrations, the combined effects of the radiolytic yield of each species due to radiation, and the changes in concentration due to chemical reactions and fluid convection, must be carefully taken into account.

Due to interaction between water molecules and neutron and gamma radiation, various molecules, ions, and radicals are created in the medium. The numbers of species " i " formed on absorption of 100 eV of energy from neutrons and gamma photons are accounted for by the parameters G_i^n and G_i^γ, respectively. Radiolytic yields (G-values) for room temperature and high temperature water are available from Burns and Moore[13] and Lukashenko et al[14], and are given in Table 1. Radiolysis is the primary source of most species in RADIOCHEM, and the rate at which any primary species is produced is given by

$$R_i^y = \left(\frac{G_i^\gamma \Gamma^\gamma}{100 N_V} + \frac{G_i^n \Gamma^n}{100 N_V}\right) \tilde{F} \rho dV \qquad (1)$$

where R_i^y has units of mol/s, Γ^n and Γ^γ are the dose rates of neutrons and gamma photons, respectively, in Rad/sec, N_V is Avogadro's number, $\tilde{F}$ equals 6.25×10^{13} (the conversion factor from Rad/sec to eV/gram-sec), ρ is the density of water in g/cm^3, and dV is the liquid phase volume increment.

The chemical reactions occurring in the heat transport circuits of BWRs essentially determine the species concentrations in each part of the circuit, particularly in regions of low dose rate (i.e. in out-of-core regions). The reaction set used in this study is given in Table 2, along with the rate constants and the activation energies. This reaction set is based on a published compilation[12], but has been modified to include hydrogen peroxide decomposition

$$H_2O_2 \rightarrow H_2O + \frac{1}{2}O_2 \qquad (2)$$

The rate of change of each species at a given location is given by elementary reaction rate theory as

$$R_i^c = \sum_{s=1}^{N}\sum_{m=1}^{N} k_{sm}\, C_s\, C_m dV - C_i \sum_{s=1}^{N} k_{si} C_s dV \qquad (3)$$

where k_{sm} is the rate constant for the reaction between Species s and m (which are the "parent" species) in the formation of Species i, k_{si} is the rate constant for the reaction between Species s and i in the destruction of i, and C_i, C_m, and C_s are the concentrations of Species i, m, and s, respectively.

The rate constant, k_j (j denotes the reaction number in Table 2), is a function of coolant temperature. Since the temperature throughout the heat transport circuit is not constant, the actual rate constant for each chemical reaction must be calculated for each specific position using Arrhenius' law

$$k_j = k_j^o \exp[\frac{E_a}{R}(\frac{1}{T_o} - \frac{1}{T})] \tag{4}$$

where k_j^o is the rate constant at temperature T_o, E_a is the activation energy, R is the universal gas constant, and T is the temperature in Kelvin. The rate constant for hydrogen peroxide decomposition (Reaction 30) was calculated separately using an experimentally derived relationship[15]:

$$k_{30} = 1.4096 \times 10^5 \cdot e^{-(\frac{14800}{RT})}. \tag{5}$$

As in all radiolysis models, we consider convection as the only mode of transport (i.e. we neglect diffusion and electromigration), and we assume that two-phase (water/steam) flow exists only in the reactor core channels. Single phase (water) flow is assumed to exist in the other regions of the circuit, such as the core bypass, upper plenum, etc. Thus, the rate of change of the number of moles of each species in volume element dV due to convection is

$$R_i^v = \frac{d(uC_i)}{dx} dV \tag{6}$$

where u is the coolant velocity in the volume increment dV.

When coolant enters the bottom of the reactor core, the temperature of the coolant starts to increase due to heat transfer from the fuel rods and by deposition of energy directly in the water by neutrons and gamma photons. After the saturation temperature is reached, steam is produced and the volume of the vapor phase expands from the point where boiling starts to the exit of the reactor core. When the vapor phase is formed, in addition to the formation of steam, mass transfer of dissolved gases occurs from the liquid phase to the vapor phase. A simplified model for describing mass transfer in two-phase flow was developed by Ibe et al[16]. The general expressions from that model for this process are given by

$$\begin{aligned} R_i^m &= (\mu_i^* C_i^g - \mu_i C_i^f) dV_g \\ R_i^{m*} &= (\mu_i C_i^f - \mu_i^* C_i^g) dV_g \end{aligned} \tag{7}$$

where dV_g is vapor phase volume increment, R_i^m is rate of change of species mole number in the liquid phase, R_i^{m*} is the corresponding quantity in the vapor phase, and μ_i^* and μ_i are the gas release coefficient and gas absorption coefficient of species i, respectively, for mass transfer between the vapor phase and the liquid phase. For want of a more comprehensive model for describing gas transfer in two-phase flow, this simplified model is used in RADIOCHEM.

General Solution

For a steady state system, the total rate of change in the concentration of each species at each location is zero. Thus,

$$\begin{aligned} &(\frac{G_i^\gamma \Gamma^\gamma}{100 N_V} + \frac{G_i^n \Gamma^n}{100 N_V}) \tilde{F} \rho dV + [\sum_{s=1}^{N} \sum_{m=1}^{N} k_{sm} C_s C_m - C_i \sum_{s=1}^{N} k_{si} C_s] dV \\ &+ [\frac{d(uC_i)}{dx} dV] \pm (\mu_i^* C_i^g - \mu_i C_i^l) dV_g = 0. \end{aligned} \tag{8}$$

Because a one-dimensional calculation only is considered in the analysis, dV can be expressed as $A(x)dx$, where $A(x)$ is the cross sectional area at a specific point x. Eq. (8) can then be rewritten by replacing dV with $[A_f(x)+A_g(x)]dx$ where A_f and A_g are the cross sectional areas of liquid and vapor, respectively. Accordingly, the steady-state for the liquid phase is described by

$$
\begin{aligned}
&(\frac{G_i^{\gamma}\Gamma^{\gamma}}{100N_V}+\frac{G_i^{n}\Gamma^{n}}{100N_V})\tilde{F}\rho_f A_f(x)dx \\
&+[\sum_{s=1}^{N}\sum_{m=1}^{N}k_{sm}C_s^f C_m - C_i^f\sum_{s=1}^{N}k_{si}C_s^f]A_f(x)dx \\
&+[u_f(x)C_i^f(x)A_f(x)-u_f(x+dx)C_i^f(x+dx)A_f(x+dx)] \\
&+(\mu_i^* C_i^g-\mu_i C_i^f)A_g(x)dx=0
\end{aligned}
\qquad (9)
$$

and that for the vapor phase by

$$
\begin{aligned}
&(\frac{G_i^{\gamma}\Gamma^{\gamma}}{100N_V}+\frac{G_i^{n}\Gamma^{n}}{100N_V})\tilde{F}\rho_g A_g(x)dx \\
&+[\sum_{s=1}^{N}\sum_{m=1}^{N}k_{sm}C_s^g C_m^g - C_i^g\sum_{s=1}^{N}k_{si}C_s^g]A_g(x)dx \\
&+[u_g(x)C_i^g(x)A_g(x)-u_g(x+dx)C_i^g(x+dx)A_g(x+dx)] \\
&+(\mu_i C_i^f-\mu_i^* C_i^g)A_g(x)dx=0
\end{aligned}
\qquad (10)
$$

where superscripts f and g represent the liquid and vapor phases, respectively, ρ_f is the density of liquid water in g/cm^3, ρ_g is the density of steam in g/cm^3, and u_f and u_g are the flow velocities in the liquid phase and in the vapor phase, respectively. Equation (10) can be further simplified by omitting the first two terms for the following reasons: Firstly, the value derived from the first term is relatively small when compared with the values of the other terms. This is mainly due to the fact that the density of steam is small. Secondly, with the assumption that the steam is dry, there are only three species, $H_2O(g)$, H_2, and O_2, in the vapor phase. Because no highly reactive radical species are present, little chemical reaction is expected over the time of residence of steam in the vessel.

Equations (9) and (10) were solved to yield species concentrations at closely spaced points around the primary heat transport circuit using an implicit trapezoidal method with Newton's algorithm for solving a system of non-linear equations. In the actual numerical simulation, all of the parameters except the flow velocity and the void fraction, in these two equations were obtained from the published literature[5,13-17]. Rate constants for the chemical reactions and the radiolytic yields for the primary species have already been given, although the rate constant of the decomposition of H_2O_2 and the gas release and absorption coefficients were employed as adjustable parameters when calibrating RADIOCHEM against an operating reactor (Dresden-2). The gas release and absorption coefficients that were determined by this procedure are shown in Table 3. A detailed discussion of the flow velocity and void fraction derivation is presented in the next section.

Heat Transfer in the Primary Circuits of BWRs

In order to solve Equations (9) and (10) for the concentration of each species in a BWR heat transport circuit, a heat transfer model is needed for calculating the void fraction distribution in the core region, and the temperature and flow velocity are required at all locations around the circuit[18,19]. At this stage of development of DAMAGE-PREDICTOR, a simplified thermal-hydraulic code, named ZEBRA,

is used for the reactor core thermal-hydraulic analysis. ZEBRA was developed Blakeslee[18] and is somewhat easier to apply than the more comprehensive codes, such as the Transient Reactor Analysis Code (TRAC-BD1/MOD1)[19]. This code (ZEBRA) calculates the temperatures of fuel, cladding, and coolant in the reactor core, if specific plant data are supplied. Furthermore, the heat transfer coefficient and steam quality versus core height are also obtained. The shortcoming of ZEBRA is that subcooled boiling is not taken into account, although homogeneous, two-phase flow is assumed in the algorithm. However, at the current stage of development of DAMAGE-PREDICTOR, ZEBRA is still useful for performing the thermal-hydraulic analysis in the BWR core. Although the flow velocity and void fraction are not provided in the output of ZEBRA, they can be calculated using Bankoff's equation[20] and mass balance.

Dose Rate Profiles of Neutron and Gamma

The importance of accurately simulating the neutron and gamma dose rates in the primary circuit, especially in the downcomer region, has been previously emphasized[1,16]. The radiolytic decomposition of water and the decomposition of hydrogen peroxide in the downcomer region are believed to be important factors in determining the oxygen concentration in the recirculation line. The dose rate profiles must be supplied for the primary heat transport circuit of the plant to be analyzed, although neutron transport codes, such as DOT-III, have been developed in the past for calculating the dose rate profiles. In the present study, the dose rate data were obtained from Reference 1.

Mixed Potential Model

After the concentration of each radical species is calculated, the corrosion potential of the component can be calculated using the Mixed Potential Model[6,7]. The MPM is based on the physical condition that charge conservation must be obeyed at the steel surface. Because electrochemical reactions transfer charge across a metal/solution interface at rates measured by the partial currents, the following equation expresses the charge conservation constraint for a uniformly accessible surface

$$\sum_{j=1}^{n} i_{R/O,j}(E) + i_{corr}(E) = 0 \qquad (11)$$

where $i_{R/O,j}$ is the partial current density due to the j-th redox couple in the system and i_{corr} is the corrosion current density of the steel substrate. These partial currents depend on the potential drop across the metal/solution interface. Details of this model may be found in the literature[2,3].

Coupled Environment Fracture Model

After the concentration of each electroactive species and the corrosion potential have been calculated , the crack growth rate of any existing crack can be estimated using the Coupled Environment Fracture Model (CEFM)[8-12].

The basic assumption of the CEFM is that crack advance occurs via the slip/dissolution/repassivation mechanism, but the governing physico-chemical condition is the conservation of charge. In the case of a crack, this condition is expressed as

$$i_{crack} A_{crack} + \int_{S} i_c^N dS = 0 \qquad (12)$$

where i_{crack} is the current density exiting the crack mouth (which may be different from that at the crack tip if cathodic reactions occur within the crack), A_{crack} is the area of the crack mouth, i_c^N is the net

(cathodic) current density due to charge transfer reactions on the external surface, S is the area of the surface outside the crack, and dS is an increment of the external surface area.

Figure 4 demonstrates the physico-electrochemical basis of the CEFM. In addition to the oxygen reduction reaction on the external surface, it is important to note that hydrogen oxidation, electrodissolution of the steel, and hydrogen peroxide reduction are also included in the CEFM. Accordingly, the net cathodic current density at any point on the external surface can then be expressed as

$$i_c^N = i(H_2) + i(O_2) + i(H_2O_2) + i_{diss} \qquad (13)$$

where $i(H_2)$, $i(O_2)$, and $i(H_2O_2)$ are the partial current densities for the redox reactions and i_{diss} is the dissolution current density of the metal.

In calculating the crack growth rate, it is necessary to estimate the crack tip strain rate. Two methods for obtaining the crack tip strain rate were employed in the present work: Ford et al's[21] empirical method and Congleton and co-workers' [22] fracture mechanics technique. Details of how these methods are incorporated into the CEFM are given elsewhere[12,23,24].

Crack growth rates calculated using the CEFM, and incorporating the two approaches for estimating the crack tip strain rate, are plotted in Figure 4 as a function of ECP and conductivity (0.1 and 0.5 μS/cm at ambient temperature). Because the crack tip parameters are poorly known, we have calibrated the CEFM against the single crack growth rate (CGR)/ECP datum shown in the figure, assuming that the ambient temperature conductivity is 0.1 μS/cm (note that the conductivity at 288 °C is much higher). In all subsequent calculations, no parameter values were changed. We have also plotted in Figure 4 representative experimental CGR/ECP data taken from Ford et al[21], as well as the Ford/Andresen[21] CGR/ECP correlations for ambient temperature conductivities of 0.1, 0.2, and 0.3 μS/cm. At very negative ECP values, the CGR becomes independent of ECP. In the CEFM, this limit is modeled[12] using the void nucleation creep model of Wilkinson and Vitek[25], whereas in the Ford/Andresen model the limit appears as a consequence of the function chosen to fit CGR versus ECP data. In any event , the CEFM, when calibrated against a single datum, provides an excellent account of the experimental data and is in good agreement with the correlations of Ford and Andresen[21], provided that ECP < 0.25 V(SHE). However, the CEFM does predict a lower dependence of CGR on conductivity than indicated by the Ford/Andresen model. In this regard, we note that the Ford/Andresen correlation was apparently established using ambient temperature conductivity data, which are only marginally relevant in describing the transport properties of the environment at the elevated temperature, particularly when hydrolyzable impurities (e.g. SO_4^{2-}, Fe^{3+}, Ni^{2+}, Cr^{3+}) are present. On the other hand, the CEFM uses the conductivity at the temperature of interest, as calculated from limiting ionic conductances, when solving for the current and potential distributions in the crack internal and external environment.

In the calculations reported here, we assume a "reference crack" of 0.5 cm length in a Type 304 stainless steel matrix, sensitized to an EPR value of 15 C/cm^2, and loaded mechanically to a stress intensity of 27.5 MPa $\cdot \sqrt{m}$. We recognize that a wide spectra exist in the crack length, degree of sensitization (EPR value), and the load (stress intensity) in an actual reactor heat transport circuit, which are not represented by the calculations reported here. However, by maintaining the above parameters constant, a clearer picture is obtained of the impact of the environment on crack growth, which is a primary goal of this work.

RESULTS AND DISCUSSION

DAMAGE-PREDICTOR was calibrated by matching the calculated oxygen concentrations in the recirculation system of Dresden-2 under HWC with the measured data, using the least square fitting

method[23]. The methodology of varying the calculated oxygen concentration is to change the gas transfer coefficients in the core boiling channels and the rate constant for the decomposition of hydrogen peroxide (Reaction 30, Table 2). We found that k_{30} had to be multiplied by a factor of ten and the gas transfer coefficients had to take on the values summarized in Table 3 in order to achieve a good fit of RADIOCHEM to the Dresden-2 recirculation system oxygen data. The same set of gas transfer coefficients, and the adjusted value for the rate constant (k_{30}), were then employed to simulate HWC in Duane Arnold[23]. Comparison of the calculated and measured[1] recirculation system oxygen levels for the two plants are given in Figures 5 and 6. In general, this unique set of gas transfer coefficients (Table 3) and the modified value for k_{30} yield an accurate simulation of the recirculation oxygen levels in these two plants that exist at opposite ends of the spectrum of plants explored by Ruiz et al[1].

In addition to oxygen in the recirculation system, the calculated concentrations of oxygen and hydrogen in the main steam line are also compared with plant data in Figure 7-10. The measured steam-line hydrogen concentration data were taken from the lower and upper bound values of the nine plants reported in Reference 1, since no hydrogen data for each individual plant are available. Again, excellent agreement is obtained, recognizing that the plant data are probably no more accurate than ±20% because of errors inherent in sampling a steam phase.

ECP data that were measured in a remote autoclave connected to the recirculation system of Duane Arnold[26] are compared with the calculated data in Figure 11 for two flow velocities. The higher flow velocity (470 cm/s) corresponds to full flow conditions in the recirculation piping system and hence cannot be taken as being representative of the autoclave sampling system. On the other hand, the lower flow velocity is thought to be representative of an autoclave taking into account thermal convection. We should note that essentially identical predictions are obtained if we assume even lower flow velocities. Accordingly, we regard the level of agreement between the calculated and plant data to be excellent, given that the hydrodynamic conditions in the autoclave, in which the ECP measurements were made, are not known (to us). Furthermore, we expect that the oxygen and hydrogen peroxide concentrations might also have changed in the sampling line and these changes could affect the ECP. These findings illustrate the need to carefully design ECP monitoring systems, so that the local hydrodynamic parameters (flow velocity, hydrodynamic diameter) are known.

ECP measurements in the core bypass of Duane Arnold[23] are also compared with calculated data in Figure 12. For feedwater hydrogen concentration less than 1.5 ppm, the ECP predicted by DAMAGE-PREDICTOR is about 40-160 (average of ~100) mV lower than the measured data. However, we point out that the ECP-measuring electrode was placed inside the local power range monitor (LPRM) housing tube. Since the hydrodynamic diameter of the LPRM tube is different from that of the core bypass, the flow velocity in the LPRM tube will also be different. Therefore, based on the previous discussion, the measured ECP values would be expected to deviate from the calculated values for the bypass shown in Figure 12. Unfortunately, the author[26] does not provide any indication of the experimental uncertainty in the measured ECP. However, based on our extensive experience in high temperature aqueous electrochemistry, we do not believe the measured ECP could be any more accurate than ±50 mV. We have indicated this level of uncertainty on the measured points plotted in Figure 12.

Some modeling calculations, which relate to the crack growth rate in the upper core bypass of Duane Arnold under HWC, were performed by Indig and Nelson[27], using measured ECP data and the Ford-Andresen model for calculating crack growth rates. Their results are compared with the data predicted by DAMAGE-PREDICTOR in Figures 13-15. Because the chemical reaction set (Table 2) employed by the GE/Harwell model is different from that used by DAMAGE-PREDICTOR, the calculated species concentrations from the two models are not expected to be in agreement. Furthermore, the crack growth rates calculated by the Ford-Andresen model were for a water conductivity of 0.15 μS/cm, which is higher than the 0.1 μS/cm considered in DAMAGE-PREDICTOR calculations. The difference in conductivity is a principal reason why the crack growth rates reported by Indig and Nelson[27] are higher than those predicted by DAMAGE-PREDICTOR. Thus, as estimated in our other work[24], a doubling of the conductivity (0.1 μS/cm to 0.2 μS/cm) at high ECP values results in an increase in the crack growth rate by a factor of 2-6. The difference is predicted to be at the lower end of

this range for lower ECP values, as the crack growth rate approaches the creep limit. Accordingly, the difference in conductivity alone probably accounts for more than half of the difference in crack growth rates indicated in Figure 15. The remaining difference is presumably due to the differences in the predicted concentrations of H_2, O_2, and H_2O_2, and to differences in the algorithms for estimating crack growth rate.

SUMMARY AND CONCLUSIONS

An algorithm (DAMAGE-PREDICTOR) is described for modeling the radiolysis, corrosion potential (ECP), and crack growth rate behaviors of components in the primary coolant circuits of Boiling Water Reactors (BWRs). The algorithm contains a deterministic model for calculating the concentrations of radiolysis products around the heat transport circuit, as a function of power level and the concentration of hydrogen in the reactor feedwater. The concentrations of hydrogen, oxygen, and hydrogen peroxide, together with thermal-hydraulic data, are used to calculate the corrosion potential via the deterministic Mixed Potential Model (MPM) and the rate of growth of a reference crack (crack length= 0.5 cm, K_I= 27.5 $MPa \cdot \sqrt{m}$, water conductivity at 25 °C= 0.1 μS/cm) is calculated through the Coupled Fracture Environment Model (CEFM) at any location within the heat transport circuit. The algorithm is initially calibrated against recirculation system oxygen levels for Dresden-2, by adjusting the rate constant for the decomposition of hydrogen peroxide, and by modifying the gas release and absorption coefficients for oxygen and hydrogen within the boiling regions in the core. Without any further parameter changes, the algorithm successfully accounts for the recirculation system oxygen levels for Duane Arnold, for the steam-line O_2 and H_2 levels reported for Dresden-2 and Duane Arnold, and for ECP data measured in remote autoclaves connected to the recirculation system of Duane Arnold. Furthermore, the algorithm successfully accounts for in-core ECP data, in Duane Arnold, all as a function of hydrogen added to the reactor feedwater ($[H_2]$=0-2 ppm). The fact that Dresden-2 and Duane Arnold display widely different responses to hydrogen water chemistry (HWC), suggests that DAMAGE-PREDICTOR, once calibrated against one plant, may be applicable to a wide spectrum of BWRs, provided that design and operating differences are properly reflected in the input data.

ACKNOWLEDGMENT

The authors would like to thank the Department of Nuclear Engineering of the Pennsylvania State University for supporting one of the authors (T. K. Yeh) during the performance of this work.

REFERENCES

1. C. P. Ruiz, et al., Modeling Hydrogen Water Chemistry for BWR Applications, EPRI NP-6386, Electric Power Research Institute, June 1989.

2. E. Ibe, et al., Journal of Nuclear Science and Technology, Vol. 23, No. 1, p. 11 (1986).

3. K. Ishigure, et al., Radiat. Phys. Chem., Vol. 29, No. 3, p. 195 (1987).

4. S. R. Lukac, Radiat. Phys. Chem., Vol. 33, No. 3, p. 223 (1989).

5. J. Chun, Modeling of BWR Water Chemistry, Master Thesis, Department of Nuclear Engineering, Massachusetts Institute of Technology, 1990.

6. D. D. Macdonald, Corrosion, Vol. 48, No. 3, p. 194 (1992).

7. D. D. Macdonald, et al., "Estimation of Corrosion Potentials in the Heat Transport Circuits of LWRs," Proceedings of the International Conference on Chemistry in Water Reactors: Operating Experience & New Developments, Nice, France, Apr. 24-27, 1994.

8. D. D. Macdonald and M. Urquidi-Macdonald, Corrosion Science, Vol. 32, p. 51 (1991).

9. D. D. Macdonald and M. Urquidi-Macdonald, Proc. 4th Int. Symp. Envir. Degr. Mat. Nucl. Power Systems - Water Reactors, NACE, Jekyll Island, GA., Aug. 6-10, 1989, p. 4-1.

10. D. D. Macdonald and M. Urquidi-Macdonald, Proc. Parkins Symp. Fund. Aspects Stress Corros. Crack., Ed. S. M. Bruemmer, E. I. Meletis, R. H. Jones, W. W. Gerberich, F. P. Ford, and R. W. Staehle, TMS, Warrendale, PA, 1992, p. 443.

11. D. D. Macdonald, M. Urquidi-Macdonald, and P. C. Lu, "The Coupled Environment Fracture Model - A Deterministic Method for Calculating Crack Growth Rates," CORROSION/94, Baltimore, MD, Feb. 28 - Mar 4, 1994, Paper No. 246.

12. P. C. Lu, M. Urquidi-Macdonald, and D. D. Macdonald, Corrosion Science, to be submitted (1995).

13. W. G. Burns and P. B. Moore, Radiation Effects, Vol. 30, p. 233 (1976).

14. M. L. Lukashenko, et al., Atomnaya Energiya, Vol. 72, No. 6, p. 570 (1992).

15. C. C. Lin, et al., Int. J. Chem. Kinetics, Vol. 23, p. 971 (1991).

16. E. Ibe, et al., Journal of Nuclear Science and Technology, Vol. 23, No. 1, p. 11 (1986).

17. D. D. Macdonald and M. Urquidi-Macdonald, Corrosion, Vol. 46, No. 5, p. 380 (1990).

18. J. A. Blakeslee, ZEBRA - A Computer Code for the Steady-State Thermal Analysis of Light Water Cooled Nuclear Power Reactor, Master Paper, Department of Nuclear Engineering, The Pennsylvania State University, 1974.

19. "TRAC-BD1/MOD1: An Advanced Best Estimate Computer Program for Boiling Water Reactor Transient Analysis," Vol. 1, TRAC-BD1/MOD1 User's Manuals.

20. J. H. Rust, Nuclear Power Plant Engineering, S. W. Holland Company, Atlanta, GA., 1979.

21. P. Ford, et al., Corrosion-Assisted Cracking of Stainless and Low-Alloy Steels in LWR Environments, Final Report, EPRI NP-5064M, February 1987.

22. J. Congleton, et al., Corrosion Science, Vol. 25, p. 633 (1985).

23. T. K. Yeh, The Viability of Hydrogen Water Chemistry for Mitigating Stress Corrosion Cracking in Boiling Water Reactor Heat Transport Circuits, Ph.D. Thesis, Department of Nuclear Engineering, The Pennsylvania State University, University Park, PA, 1994.

24. T. K. Yeh, D. D. Macdonald, and A. T. Motta, "Modeling Water Chemistry, ECP, and Crack Growth Rate in the BWR Heat Transport Circuits", To be submitted to Nuclear Science & Engineering, 1994.

25. D. S. Wilkinson and V. Vitek, Acta Metall., Vol. 30, p. 1723 (1982).

26. M. E. Indig, "Recent Advances in Measuring ECPs in BWR Systems," Proc. 4th Intl. Symposium on Environmental Degradation of Materials in Nuclear Power Systems - Water Reactors, NACE, Jekyll Island, GA., Aug. 6-10, 1989, p. 4-411.

27. M. E. Indig and J. L. Nelson, Corrosion, Vol. 47, No. 3, p. 202 (1991).

Table 1
G Values for Primary Radiolytic Species in Water at 25 °C and 285 °C

		25 °C		285 °C	
No.	Species	G^n	G^γ	G^n	G^γ
1	e^-	0.93	2.70	1.08	4.15
2	H	0.50	0.61	0.66	1.08
3	H^+	0.93	2.70	1.08	4.15
4	OH	1.09	2.86	0.26	3.97
5	OH^-	0.00	0.00	0.00	0.00
6	H_2O_2	0.99	0.61	0.74	1.25
7	HO_2	0.04	0.03	0.00	0.00
8	HO_2^-	0.00	0.00	0.00	0.00
9	O_2	0.00	0.00	0.00	0.00
10	O_2^-	0.00	0.00	0.00	0.00
11	H_2	0.88	0.43	0.00	0.62

Table 2
Chemical Reaction Set Employed in RADIOCHEM

No.	Chemical Reactions	Rate Constant (25 C) (L/mol-sec)	Activation Energy (Kcal/mol)
1	$e^- + H_2O = H + OH^-$	1.6×10^0	3.0
2	$e^- + H^+ = H$	2.4×10^{10}	3.0
3	$e^- + OH = OH^-$	2.4×10^{10}	3.0
4	$e^- + H_2O_2 = OH + OH^-$	1.3×10^{10}	3.0
5	$H + H = H_2$	1.0×10^{10}	3.0
6	$e^- + HO_2 = HO_2^-$	2.0×10^{10}	3.0
7	$e^- + O_2 = O_2^-$	1.9×10^{10}	3.0
8	$2e^- + 2H_2O = 2OH^- + H_2$	5.0×10^9	3.0
9	$2OH + H_2O = H_2O_2$	4.5×10^9	3.0
10	$OH + HO_2 = H_2O + O_2$	1.2×10^{10}	3.0
11	$OH + O_2^- = OH^- + O_2$	1.2×10^{10}	3.0
12	$OH^- + H = e^- + H_2O$	2.0×10^7	4.5
13	$e^- + H + H_2O = OH^- + H_2$	4.5×10^8	3.0
14	$e^- + HO_2^- + H_2O = OH + 2OH^-$	6.3×10^7	3.0
15	$H^+ + OH^- = H_2O$	1.44×10^{11}	3.0
16	$H_2O = H^+ + OH^-$	2.6×10^{-5}	3.0
17	$H + OH = H_2O$	2.0×10^{10}	3.0
18	$OH + H_2 = H + H_2O$	3.4×10^7	4.6
19	$OH + H_2O_2 = H_2O + HO_2$	2.7×10^7	3.45
20	$H + H_2O_2 = OH + H_2O$	4.4×10^7	4.5
21	$H + O_2 = HO_2$	1.9×10^{10}	3.0
22	$HO_2 = O_2^- + H^+$	8.0×10^5	3.0
23	$O_2^- + H^+ = HO_2$	5.0×10^{10}	3.0
24	$2HO_2 = H_2O_2 + O_2$	2.7×10^6	4.5
25	$2O_2^- + 2H_2O = H_2O_2 + O_2 + 2OH^-$	1.7×10^7	4.5
26	$H + HO_2 = H_2O_2$	2.0×10^{10}	3.0
27	$H + O_2^- = HO_2^-$	2.0×10^{10}	3.0
28	$e^- + O_2^- = HO_2^- + OH^-$	1.3×10^8	4.5
29	$OH^- + H_2O_2 = HO_2^- + H_2O$	1.8×10^8	4.5
30	$H_2O_2 = H_2O + 1/2\ O_2$	0.2	N. A.
31	$H + H_2O = H_2 + OH$	1.04×10^{-4}	3.0
32	$H_2O + HO_2^- = H_2O_2 + OH^-$	1.02×10^4	3.0
33	$HO_2 + O_2^- = O_2 + HO_2^-$	1.5×10^7	4.5
34	$H_2O_2 = 2OH$	7.7×10^{-4}	7.3

Table 3
Gas Release and Absorption Coefficients for Hydrogen and Oxygen

Coefficient	O_2	H_2
Gas Release μ (s^{-1})	228	255
Gas Absorption μ^* (s^{-1})	21.5	15.0

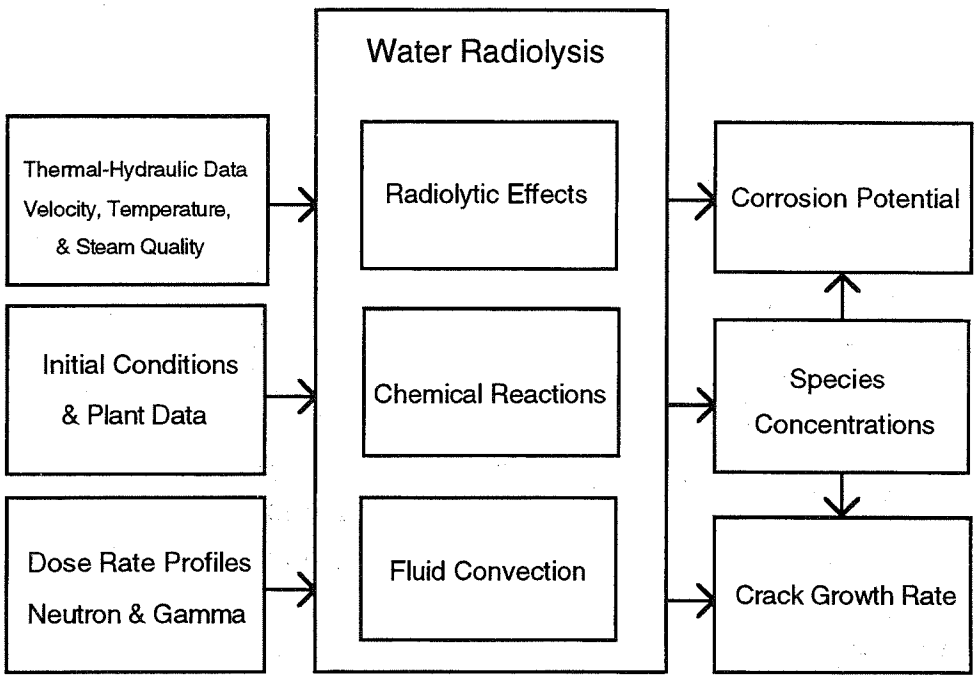

Figure 1. Structure of the DAMAGE-PREDICTOR algorithm.

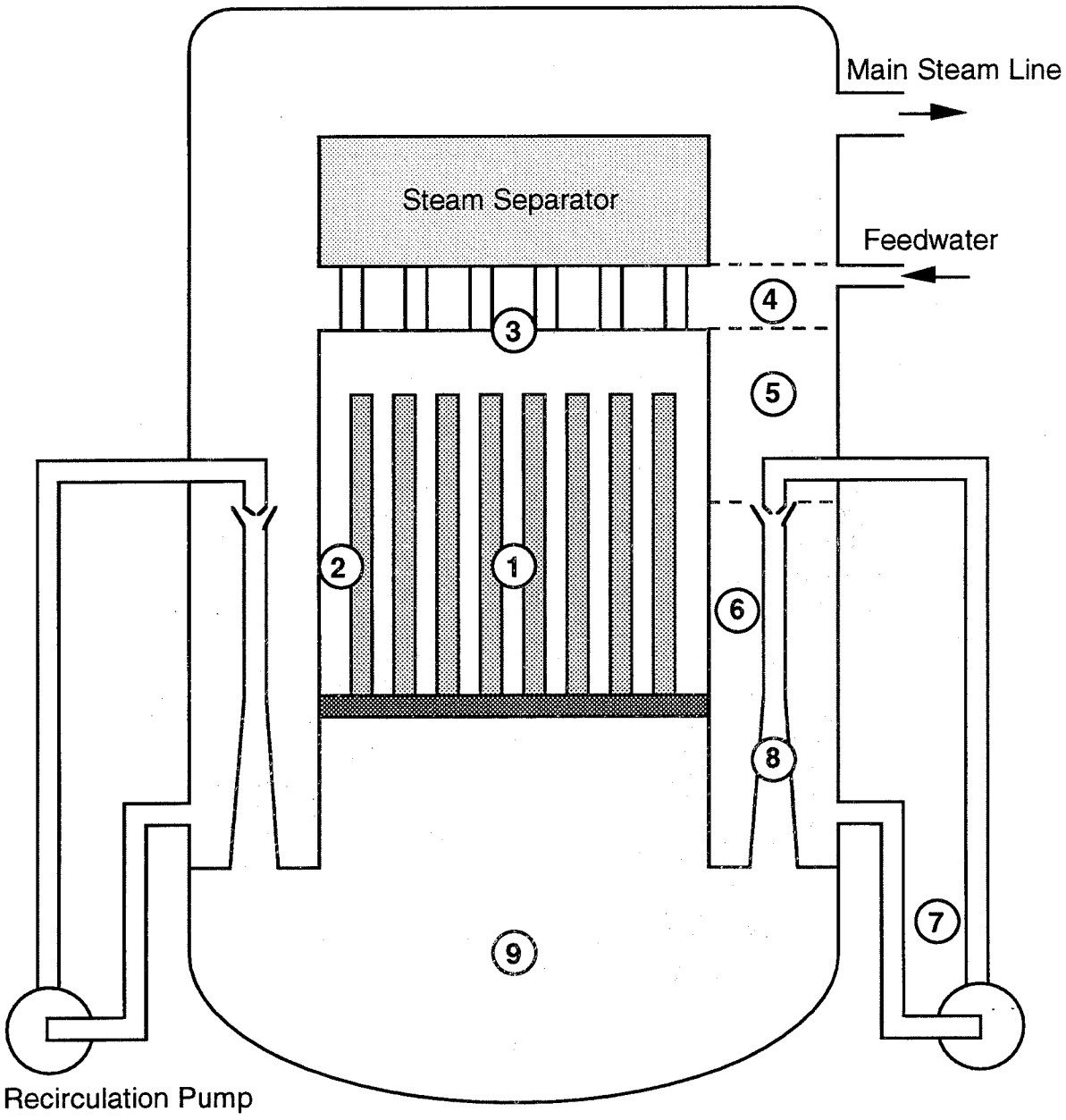

1. Core Channel
2. Core Bypass
3. Upper Plenum
4. Mixing Plenum
5. Upper Downcomer
6. Lower Downcomer
7. Recirculation Line
8. Jet Pump
9. Lower Plenum

Figure 2. Conceptual configuration of a typical BWR heat transport circuit.

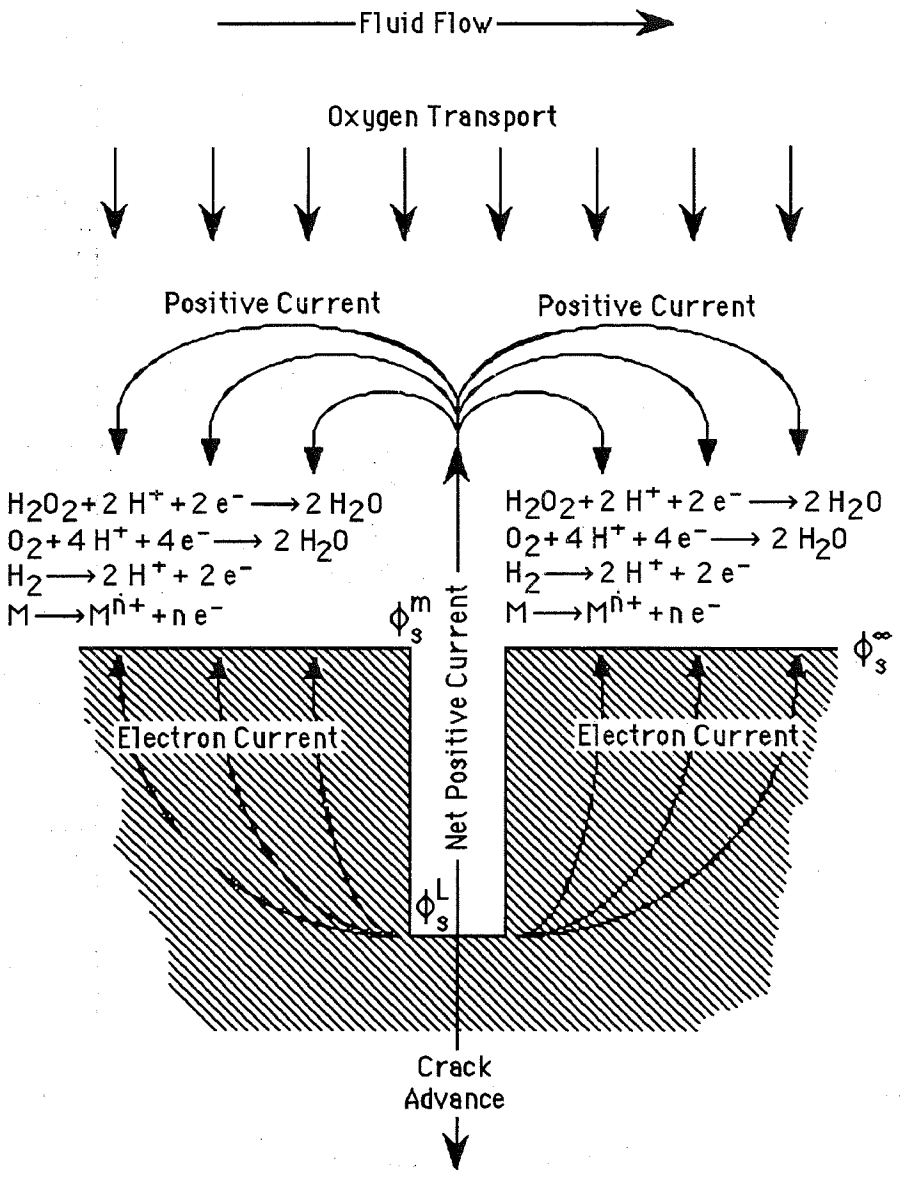

Figure 3. Illustration of theoretical basis for the CEFM. The potentialsThe potentials, ϕ_s^L, ϕ_s^m, and ϕ_s^∞, are the electrostatic potentials in the solution adjacent to the crack tip, at the crack mouth, and adjacent to a remote point on the external surface, respectively. The aspect ratio of the crack is assumed to be sufficiently large that the internal crack environment is quiescent.

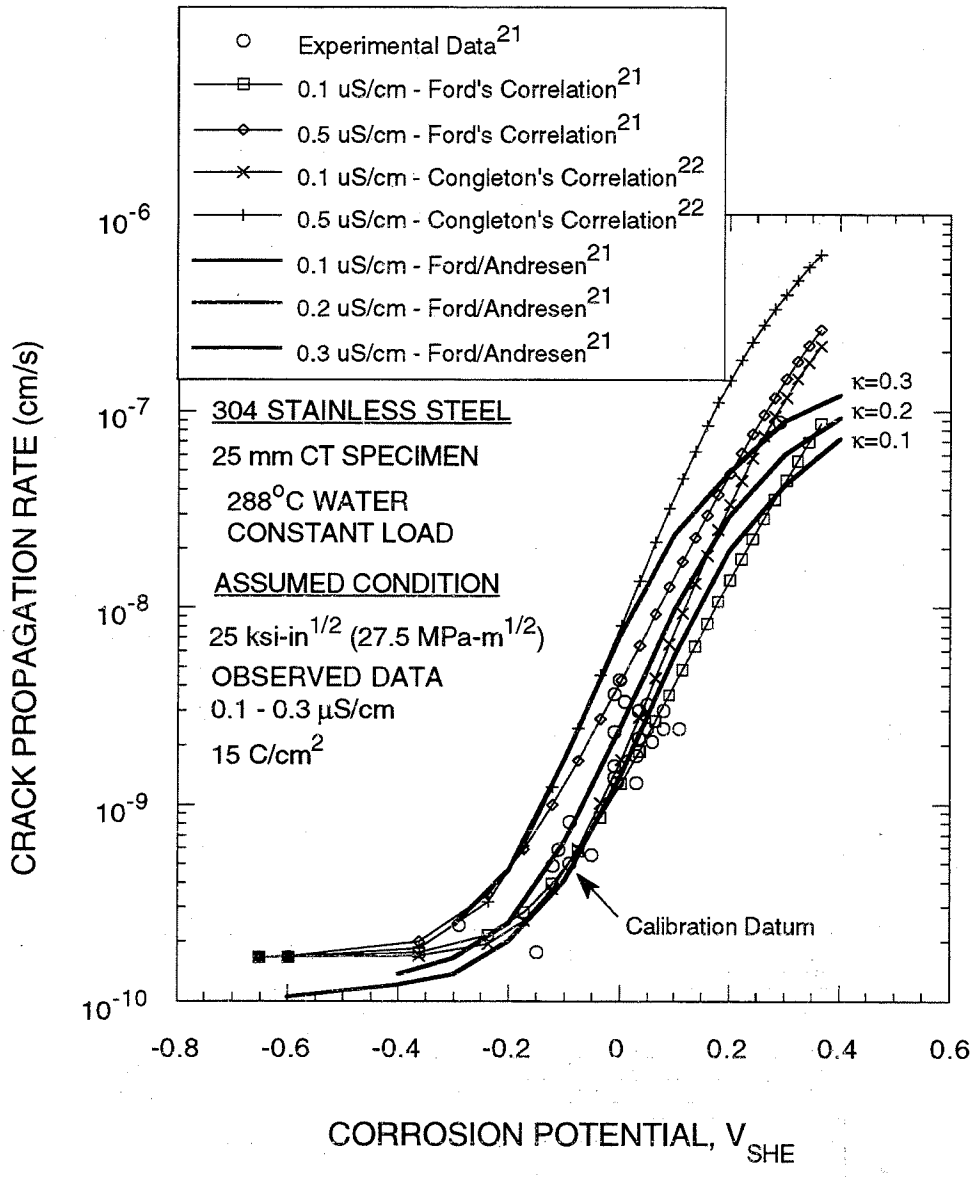

Figure 4. Measured and calculated (using the CEFM) crack growth rate of sensitized Type 304 stainless steel as a function of corrosion potential. The Ford/Andresen[21] correlations, which were derived from a multivariate empirical model that was fit to various experimental data are included for comparison. Although the actual data base used by Ford and Andresen apparently has not been published, some of the experimental data contained in this plot are believed to be from that data base.

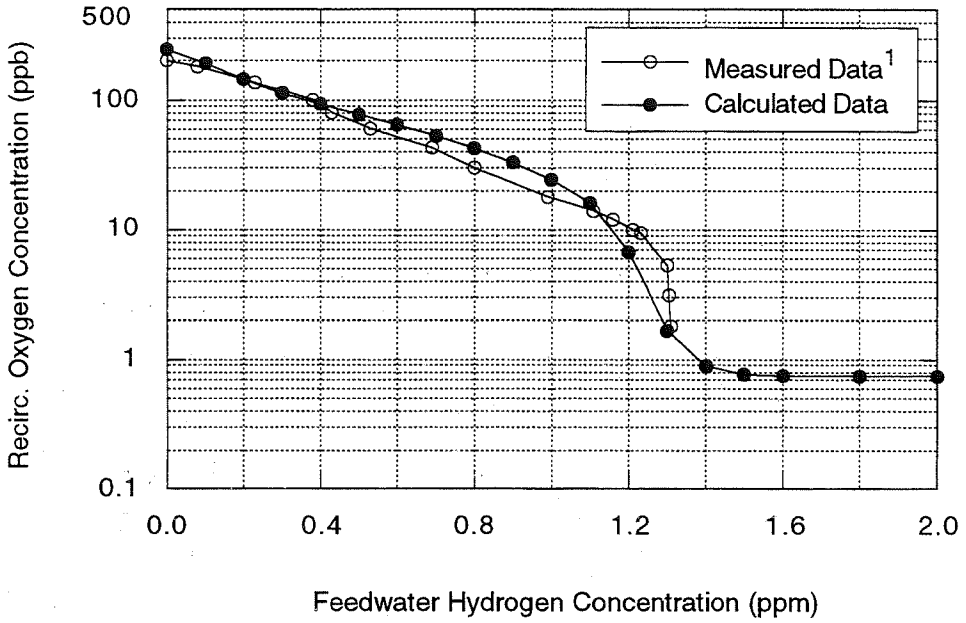

Figure 5. Effect of hydrogen addition on the oxygen concentration in the recirculation system exit of Dresden-2. Note that the measured data[1] were used to calibrated DAMAGE-PREDICTOR using a least squares method, in which the gas absorption and release coefficients for H_2 and O_2 in the core and the rate constant for H_2O_2 decomposition were employed as fitting parameters.

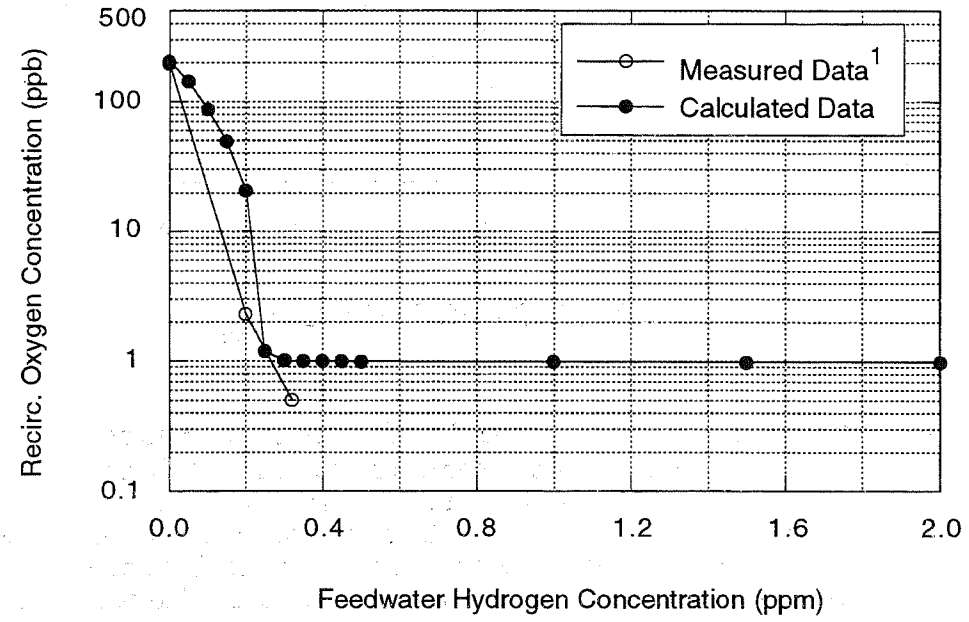

Figure 6. Effect of hydrogen addition on the oxygen concentration in the recirculation system exit of Duane Arnold. The calculated data were obtained using the same values for the gas absorption and release coefficients for H_2 and O_2 in the reactor core and the same rate constant for H_2O_2 decomposition as employed in Figure 5.

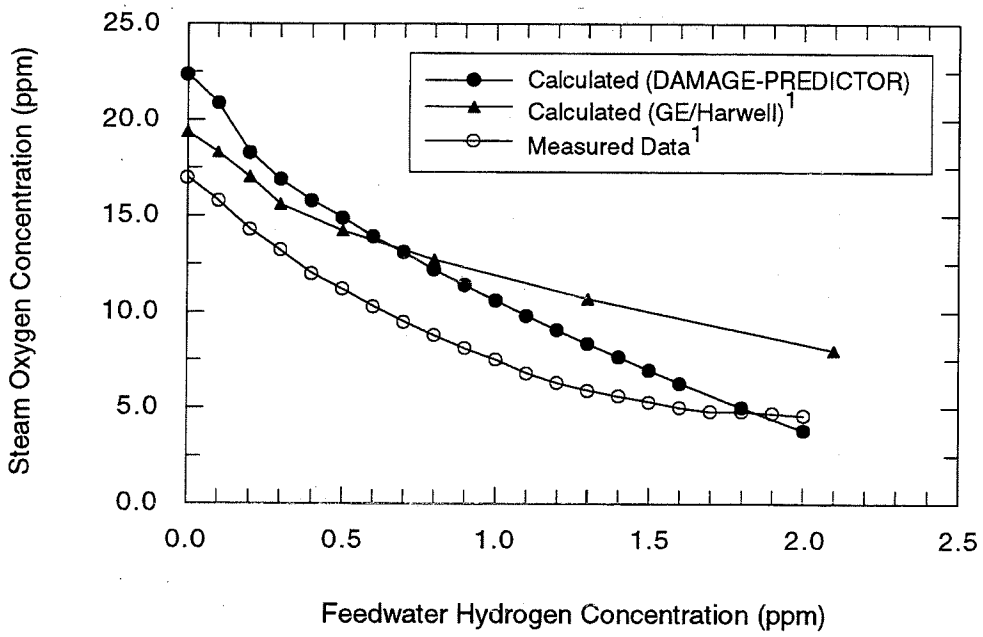

Figure 7. Oxygen variations in the main steam line of Dresden-2 due to added hydrogen. The calculated data were obtained using the same values for the gas absorption and release coefficients for H_2 and O_2 in the reactor core and the same rate constant for H_2O_2 decomposition as employed in Figure 5.

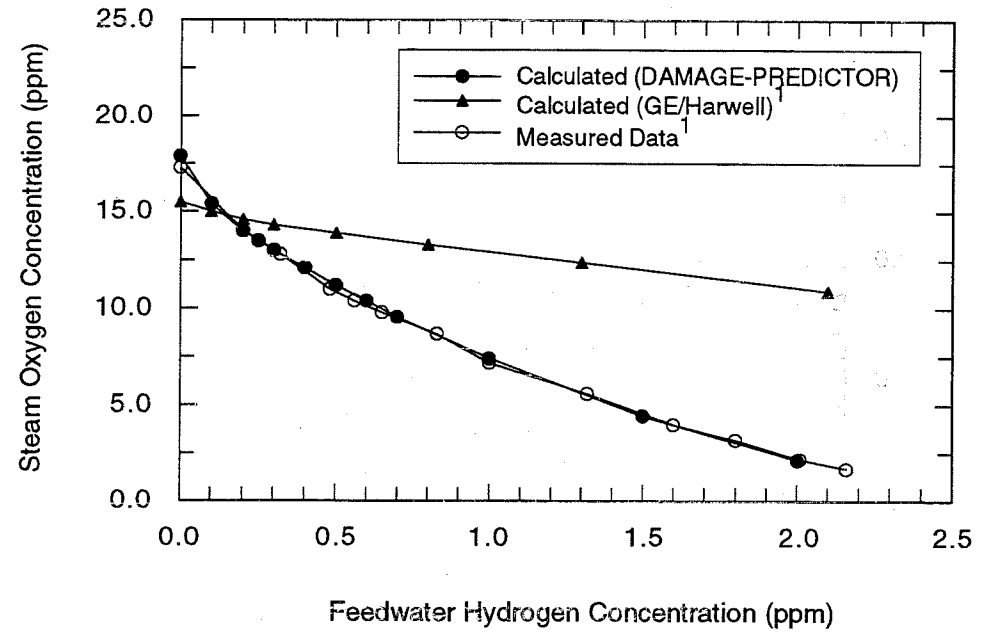

Figure 8. Oxygen variations in the main steam line of Duane Arnold due to added hydrogen. The calculated data were obtained using the same values for the gas absorption and release coefficients for H_2 and O_2 in the reactor core and the same rate constant for H_2O_2 decomposition as employed in Figure 5.

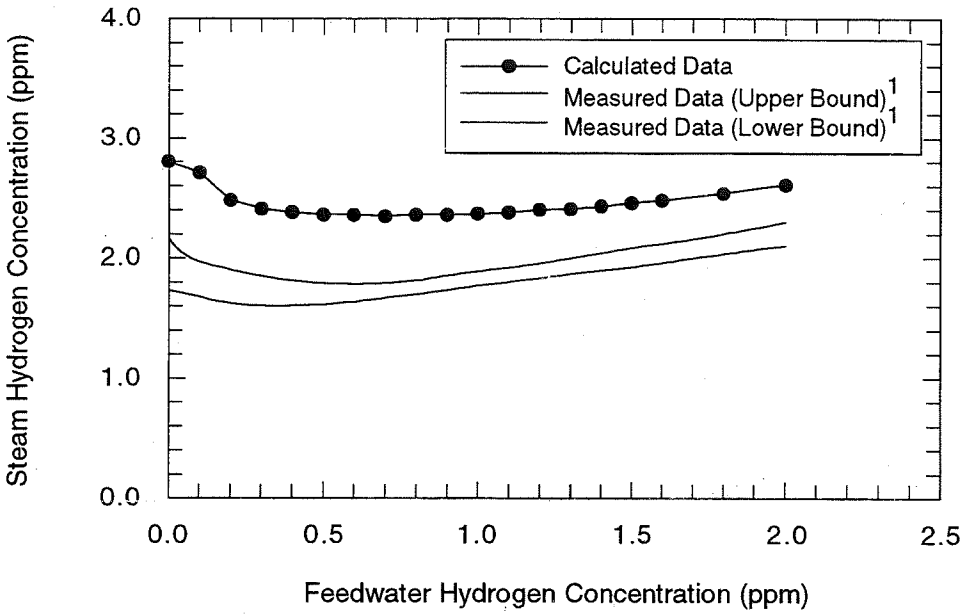

Figure 9. Hydrogen variations in the main steam line of Dresden-2 due to added hydrogen. The calculated data were obtained using the same values for the gas absorption and release coefficients for H_2 and O_2 in the reactor core and the same rate constant for H_2O_2 decomposition as employed in Figure 5.

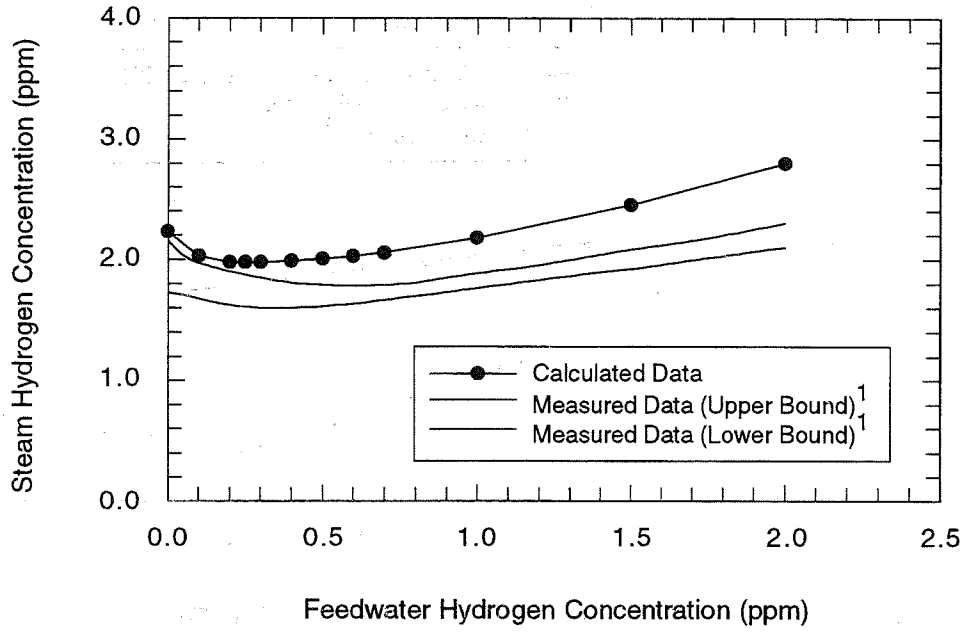

Figure 10. Hydrogen variations in the main steam line of Duane Arnold due to added hydrogen. The calculated data were obtained using the same values for the gas absorption and release coefficients for H_2 and O_2 in the reactor core and the same rate constant for H_2O_2 decomposition as employed in Figure 5.

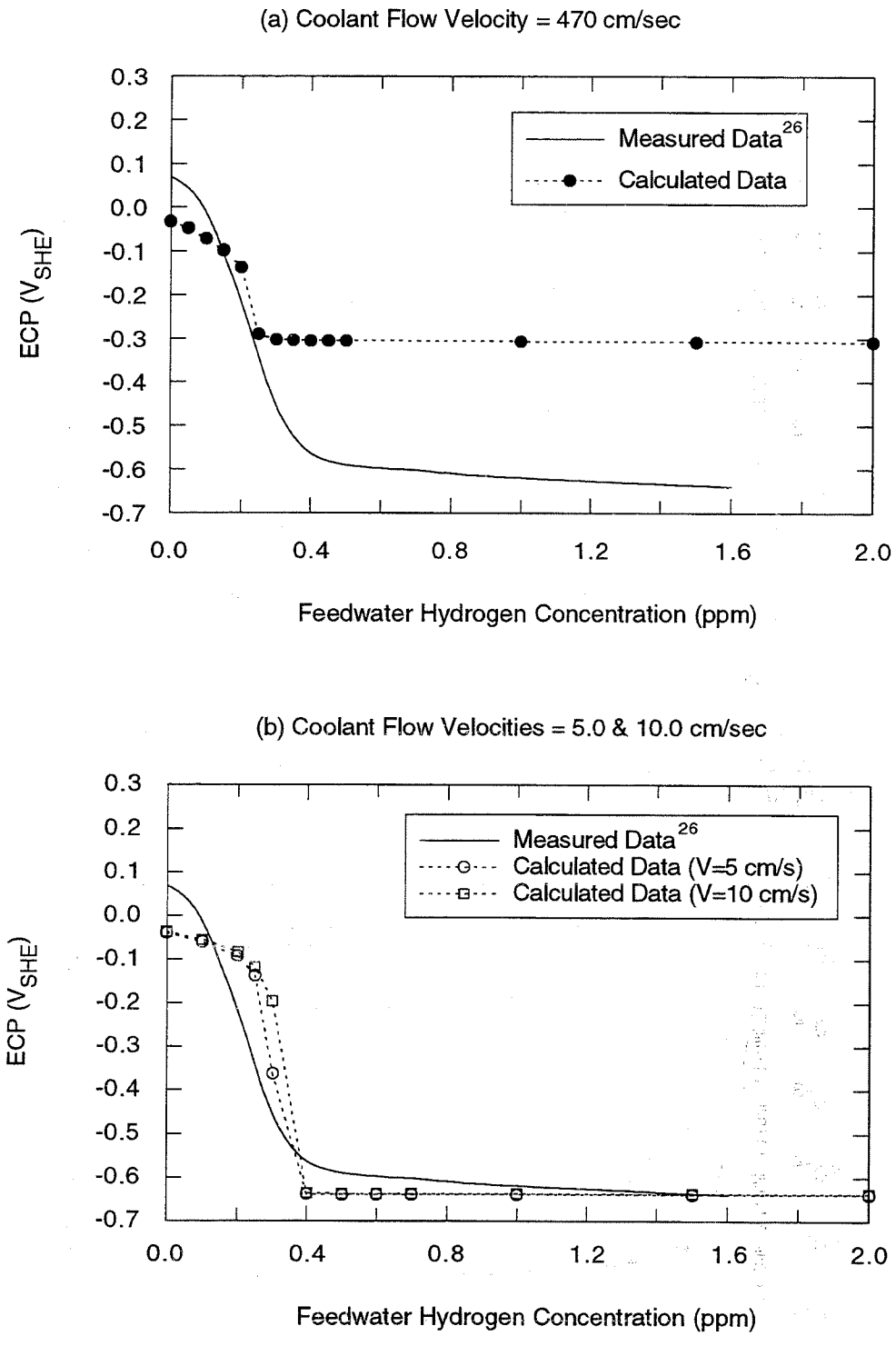

Figure 11. Comparison of measured (remote autoclave) and calculated ECP variations at different flow velocities for Duane Arnold under HWC. Note that the calculated ECP plotted in (a) corresponds to the recirculation piping system under normal operating conditions, whereas that plotted in (b) corresponds to conditions that are thought to exist in the remote monitoring autoclave that was connected to the recirculation system. The calculated data were obtained using the same values for the gas absorption and release coefficients for H_2 and O_2 in the reactor core and the same rate constant for H_2O_2 decomposition as employed in Figure 5.

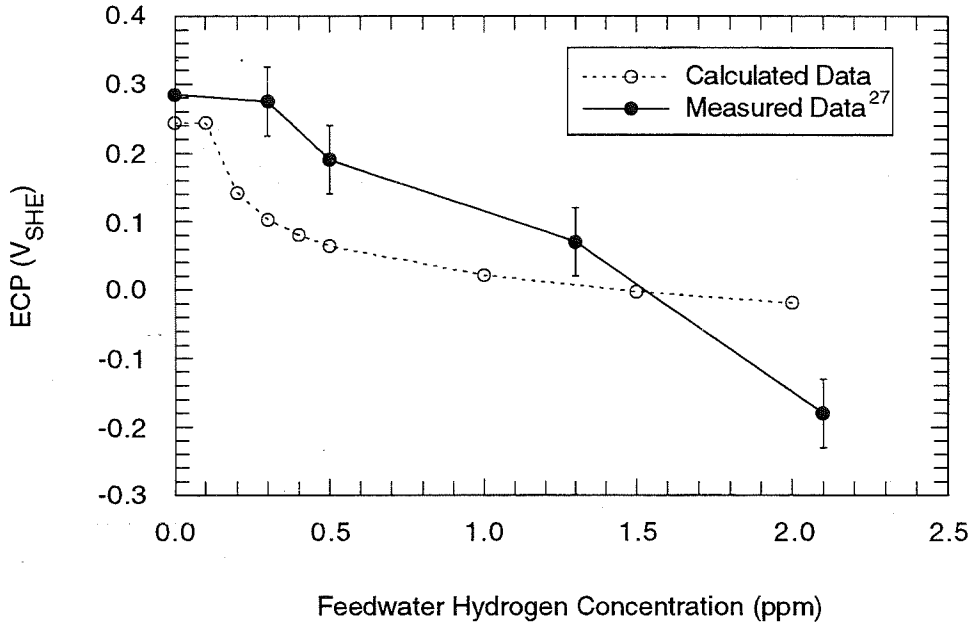

Figure 12. Comparison of measured and calculated ECP variations in the upper core bypass of Duane Arnold under HWC. The calculated data were obtained using the same values for the gas absorption and release coefficients for H_2 and O_2 in the reactor core and the same rate constant for H_2O_2 decomposition as employed in Figure 5.

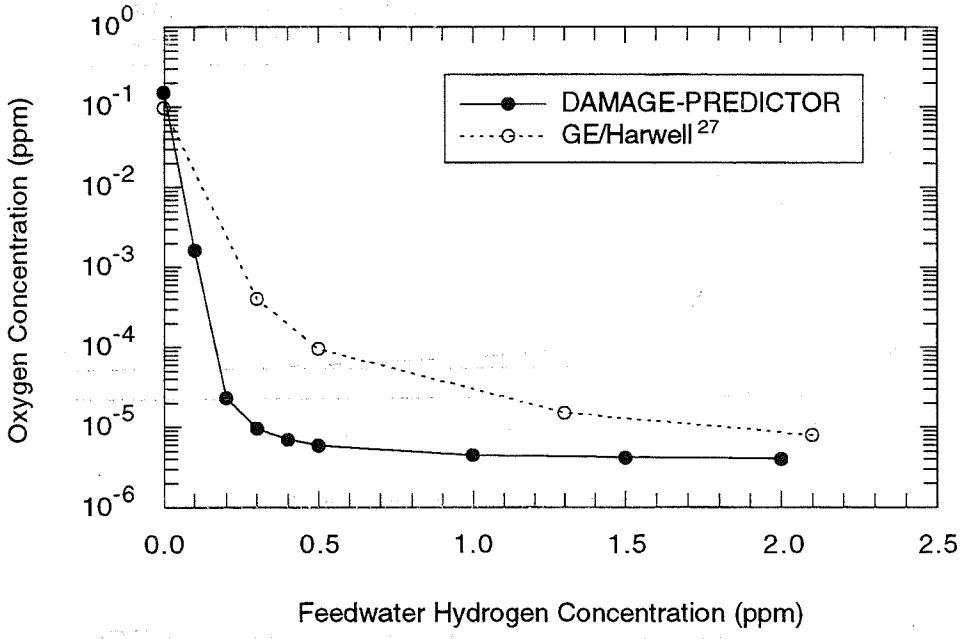

Figure 13. Comparison of calculated oxygen concentrations by DAMAGE-PREDICTOR and the GE/Harwell model in the upper core bypass of Duane Arnold under HWC. The data calculated using DAMAGE-PREDICTOR were obtained using the same values for the gas absorption and release coefficients for H_2 and O_2 in the reactor core and the same rate constant for H_2O_2 decomposition as employed in Figure 5.

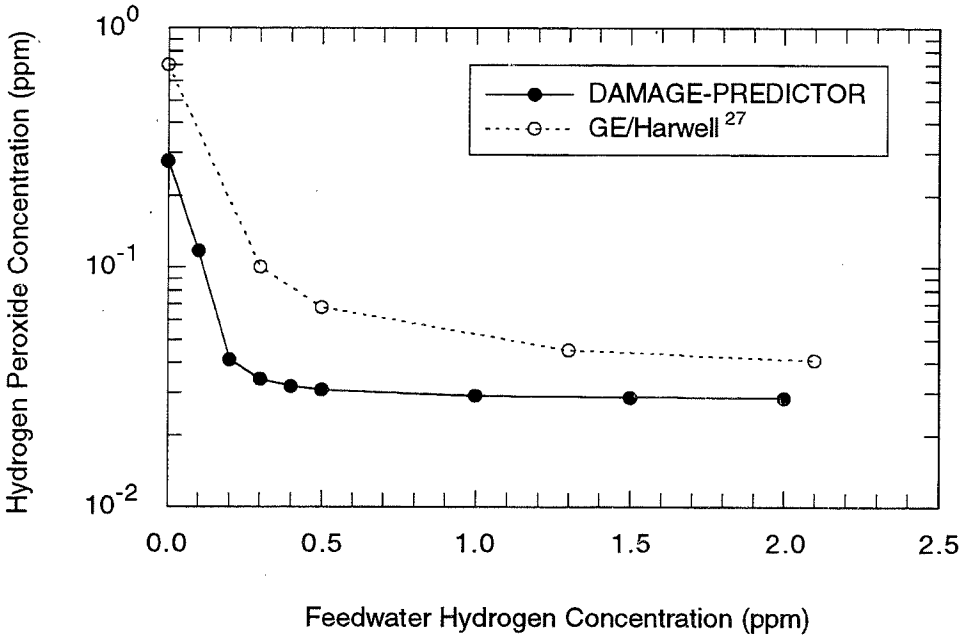

Figure 14. Comparison of calculated hydrogen peroxide concentrations by DAMAGE-PREDICTOR and the GE/Harwell model in the upper core bypass of Duane Arnold under HWC. The data calculated using DAMAGE-PREDICTOR were obtained using the same values for the gas absorption and release coefficients for H_2 and O_2 in the reactor core and the same rate constant for H_2O_2 decomposition as employed in Figure 5.

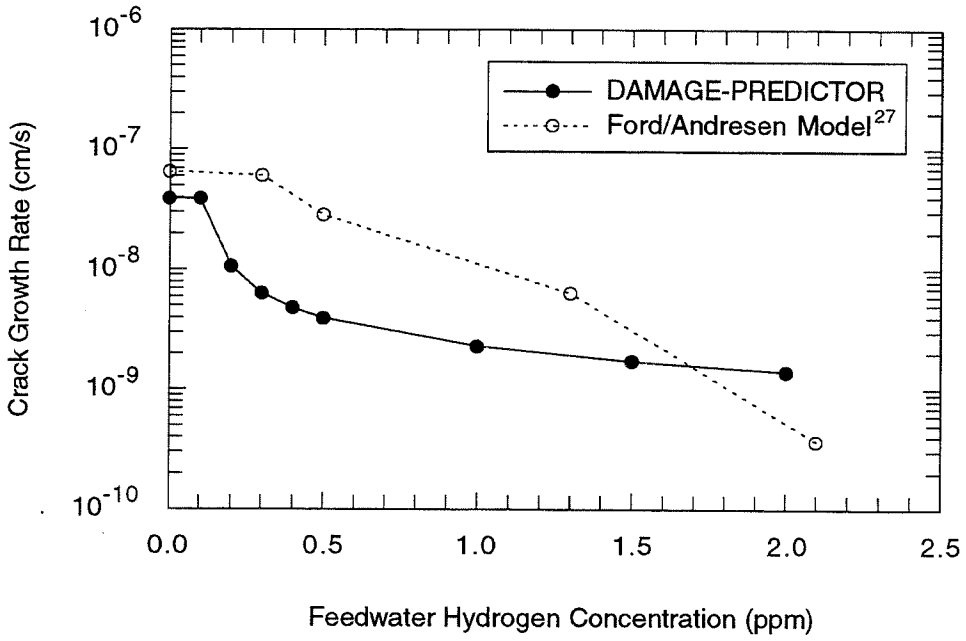

Figure 15. Comparison of calculated crack growth rates by DAMAGE-PREDICTOR and by the Ford/Andresen model using measured ECP data for upper core bypass of Duane Arnold under HWC. The data calculated using DAMAGE-PREDICTOR were obtained using the same values for the gas absorption and release coefficients for H_2 and O_2 in the reactor core and the same rate constant for H_2O_2 decomposition as employed in Figure 5.